


 CrossMark
click for updates

 Cite this: *CrystEngComm*, 2016, 18, 3703

Synthesis of Cu–Sb–S nanocrystals: insight into the mechanism of composition and crystal phase selection†

 Qingshuang Liang,^a Keke Huang,^a Xiaoru Ren,^a Wei Zhang,^b Renguo Xie^c and Shouhua Feng^{*a}

In this work, Cu–Sb–S nanocrystals (NCs) with various compositions and crystal structures are realized by only tuning the amount of 1-dodecanethiol (DDT). When the DDT amount is 3.6, 5.5, 20.5, and 25.6 mmol, pure tetragonal Cu₃SbS₄, cubic Cu₁₂Sb₄S₁₃, orthorhombic CuSbS₂, and orthorhombic Cu₃SbS₃ NCs are respectively obtained. Systematic investigations demonstrate that different amounts of DDT are responsible for formation of the different compositions and crystal structures of the initial Cu_{2–x}S seeds, which results into the formation of various Cu–Sb–S NCs. This reaction path is further verified by control experiments from successful preparation of Cu–Sb–S NCs comparable to that of the as-prepared ones directly from the reaction of Sb₂S₃ NCs with Cu_{2–x}S seeds. The current study not only provides a facile and economical way to synthesize high-quality Cu–Sb–S NCs, but also opens a new route for preparation other I–V–II multicomponent chalcogenides NCs, such as Cu–Bi–S systems.

 Received 1st March 2016,
Accepted 5th April 2016

DOI: 10.1039/c6ce00474a

www.rsc.org/crystengcomm

Introduction

Copper-based multi-component chalcogenides have received considerable interest because of their high absorption coefficients, earth-abundant compositions, and low toxicity.^{1–6} Among these copper-based materials, the copper-antimony-sulfide system, with four different phases (CuSbS₂, Cu₃SbS₃, Cu₁₂Sb₄S₁₃, and Cu₃SbS₄), have gained great attention for their potential application in supercapacitors and scalable photovoltaics.^{7–16} The different components and crystal structures of these four phases lead to great differences in terms of the electronic structures and potential applications.^{17–21} For instance, several studies have found that CuSbS₂ has an indirect band gap with low hole mobility,^{17,20,22,23} suggesting that it may not provide the optimal carrier properties for use in solar cells; however, its layer structure, with good ionic conductivity, make it attractive for energy storage applications.^{9,12} Cu₃SbS₃, which has a direct and suitable band gap, has been considered as a promising absorber material for sustainable and scalable thin-film solar cells.^{19,22,24,25} Therefore, achieving composition and phase-controlled synthesis of

Cu–Sb–S nanocrystals (NCs) is important for the use of them in any type of device.

In conventional bulk Cu–Sb–S materials synthesis, mix-phase structures are always obtained because of the very narrow thermodynamic stability window.²⁶ Colloidal chemical solution-based synthesis of semiconductor inorganic nanocrystals has been well developed in the last few decades.^{27,28} The ability to manipulate the nucleation and kinetic growth of the nanocrystals has made composition and phase-controlled syntheses possible.^{29–31} In a Cu–Sb–S system, colloidal chemistry synthesis of phase-pure Cu–Sb–S NCs has been reported.^{7,22,32–35} Tachibana *et al.* first reported the synthesis of monodisperse Cu₃SbS₄ NCs using bis(trimethylsilyl)sulfide as sulfur source.⁷ By reducing the amount of bis(trimethylsilyl)sulfide and increasing the reaction temperature, monodisperse Cu₁₂Sb₄S₁₃ NCs were also prepared.³² Using a method of thermo-decomposition of a single-source precursor, Wang *et al.* successfully synthesized rectangular CuSbS₂ nanosheets (NSs), trigonal-pyramidal Cu₁₂Sb₄S₁₃ NCs, and rhombic Cu₃SbS₃ NSs, respectively.³³ Gupta *et al.*²² reported the selective synthesis of phase-pure Cu–Sb–S NCs of all four phases by careful selection of metal, sulfide precursors, and experimental conditions. The reaction parameters, such as reaction temperature, precursor type and ratios, and ligand composition, are found to be significantly important in obtaining phase-pure Cu–Sb–S NCs.^{22,32–34} However, due to various reaction procedures and repeatability, reaction parameters for the formation of phase-pure Cu–Sb–S NCs are sometimes controversial in the literature. Knowledge of

^a State Key Laboratory of Inorganic Synthesis and Preparative Chemistry, College of Chemistry, Jilin University, Changchun 130012, PR China.

E-mail: shfeng@jlu.edu.cn; Fax: +86 431 85168624; Tel: +86 431 85168661

^b Key Laboratory of Mobile Materials, Department of Materials Science, Jilin University, Changchun 130012, PR China

^c College of Chemistry, Jilin University, Changchun 130012, PR China

† Electronic supplementary information (ESI) available. See DOI: 10.1039/c6ce00474a

composition and phase-controlled synthesis of Cu–Sb–S NCs is still unclear, which lead us to explore of the formation pathway and phase selectivity mechanism of Cu–Sb–S NCs.

In this report, we perform the phase selective synthesis of Cu–Sb–S NCs by systematic investigation of reaction parameters, such as capping agents, and the reactivity of sulfur precursors. By only tuning the amount of DDT, all four of phase-pure Cu–Sb–S NCs are obtained. The effect of the amount of DDT is studied in detail. The different amounts of DDT greatly influence the composition and crystal structure of the initial Cu_{2-x}S seeds. The formation mechanism of NCs has been proved to be reasonable because the Cu–Sb–S NCs with different compositions and crystal structures are obtainable by the reaction of Sb_2S_3 NCs with different Cu_{2-x}S seeds. Furthermore, we find that the phase structures of Cu_{2-x}S seeds can also be affected by the reactivity of the sulfur precursor, leading to phase selective synthesis of Cu–Sb–S NCs. This study on phase selectivity mechanism could be extended to the synthesis of other I–V–VI multi-component chalcogenides NCs, such as the Cu–Bi–S system.

Experimental section

Chemicals

Copper(II) acetate ($\text{Cu}(\text{Ac})_2$, 98%), 1-dodecanethiol (DDT, 98%), and 1-octadecene (ODE, 90%) were purchased from Alfa Aesar. Oleic acid (OA, 98%) and sulfur powder (99.5%) were obtained from Aladdin. Antimony chloride (99.5%) and hexane (analytical reagent) were purchased from Sinopharm Chemical Reagent Co., Ltd. Ethanol (analytical reagent) was obtained from Beijing chemical works. All chemicals were used as received without further purification.

Preparation of sulfur precursor

The sulfur precursors were obtained by dissolving 4.4 mmol sulfur powder in 5 mL ODE under argon atmosphere at 120 °C followed by heating at different temperatures (200 °C, 180 °C, and 150 °C) for 20 min.

Synthesis of Cu–Sb–S nanocrystals

The synthesis of Cu–Sb–S nanocrystals was carried out in ODE by the hot-injection method. In a typical synthesis, 1 mmol $\text{Cu}(\text{Ac})_2$ (0.1816 g), 1 mmol SbCl_3 (0.2281 g), 1 mL DDT, 2 mL OA, and 7 mL ODE were loaded into a 100 mL three-neck flask attached with a Schlenk line. The flask was degassed by a vacuum pump for 30 min to remove water and other low-boiling point impurities at 120 °C. Then, the temperature was increased to 200 °C in 10 min under an argon atmosphere. The as-prepared sulfur precursor was quickly injected and the temperature was maintained at 200 °C for 1 hour with continuous vigorous stirring. After the mixture was cooled to room temperature, 5 mL of hexane and 25 mL of ethanol were added, and the mixture was sonicated for 5 min to remove all the free ligands and the unreacted precursors. The solution was centrifuged at 8000 rpm for 5 min. The upper liquid layer was decanted and the iso-

lated solid was dispersed in hexane and re-precipitated by adding ethanol. Centrifugation and precipitation was repeated three times and the final products were re-dispersed in hexane or dried under vacuum for further measurements.

Characterization

X-ray power diffraction (XRD) patterns were recorded on a Rigaku D/Max 2500V/PC X-ray diffractometer with graphite monochromic $\text{Cu K}\alpha$ radiation ($\lambda = 0.1518$ nm). Transmission electron microscopy (TEM) and high-resolution transmission electron microscopy (HRTEM) images were taken with a FEI Tecnai G2 S-Twin F20 with an accelerating voltage of 200 kV. The sample for TEM analysis was prepared by placing a drop of the NCs hexane solution on a carbon-coated copper grid and letting it air dry. The compositions of the as-prepared Cu–Sb–S NCs were determined quasi-quantitatively by a Helios NanoLab 600I from FEI Company, at an acceleration voltage of 20 kV. X-ray photoelectron spectroscopy (XPS) was carried out with a Thermo ESCALab 250 analyzer operating at constant analyzer energy mode. The optical property measurements were performed on a U4100 UV-vis spectrophotometer equipped with an integrating sphere attachment using the as-prepared dry powders of the NCs.

Results and discussion

Cu–Sb–S nanocrystals were synthesized by a hot-injection procedure. Given that SbCl_3 has very low affinity to DDT, and $\text{Cu}(\text{Ac})_2$ is unable to dissolve in OA, the combination of DDT and OA is a good choice for balancing the reactivity of the precursors. After fixing the reaction temperature, precursor ratios and other parameters, we found that by only tuning the amounts of DDT, all four phase-pure Cu–Sb–S NCs could be obtained.

Fig. 1a shows the typical TEM image of NCs prepared with 3.6 mmol DDT. The as-prepared NCs show irregular to tetragonal shapes an average size of 61 ± 19 nm. In the HRTEM image (Fig. 1b), the observed lattice spacings of 0.31, 0.38, and 0.48 nm could be assigned to the $(\bar{1}12)$, (110), and (101) planes of tetragonal Cu_3SbS_4 , respectively. The acute angles between the planes were 90° and 50.7°, respectively. The XRD result in Fig. 1c shows that all the diffraction peaks from the product can be indexed to tetragonal Cu_3SbS_4 (PDF card No. 71-0555), thereby illustrating the pure phase of the obtained NCs. Increasing DDT to 4 mmol, little XRD peaks appear, and these peaks could be indexed to $\text{Cu}_{12}\text{Sb}_4\text{S}_{13}$ (Fig. S1†). Further increasing the DDT amount to 5.5 mmol results the preparation of phase-pure $\text{Cu}_{12}\text{Sb}_4\text{S}_{13}$ NCs. The XRD pattern in Fig. 1f corresponds to cubic $\text{Cu}_{12}\text{Sb}_4\text{S}_{13}$ (PDF card No. 88-0282). The TEM micrograph (Fig. 1d) shows that the cube nanocrystals have an average size of 140 ± 23 nm. The HRTEM image of the as-prepared NCs (Fig. 1e) shows the perfect single crystal structure of $\text{Cu}_{12}\text{Sb}_4\text{S}_{13}$ NCs. The observed interplanar distances of 0.30, 0.42, and 0.33 nm correspond to the (222), $(\bar{1}\bar{1}\bar{2})$, and (310) planes of cubic $\text{Cu}_{12}\text{Sb}_4\text{S}_{13}$, respectively. The observed acute angles also agree well with theoretical values. When the amount of DDT was in the range of 6–19 mmol, mixed-phases

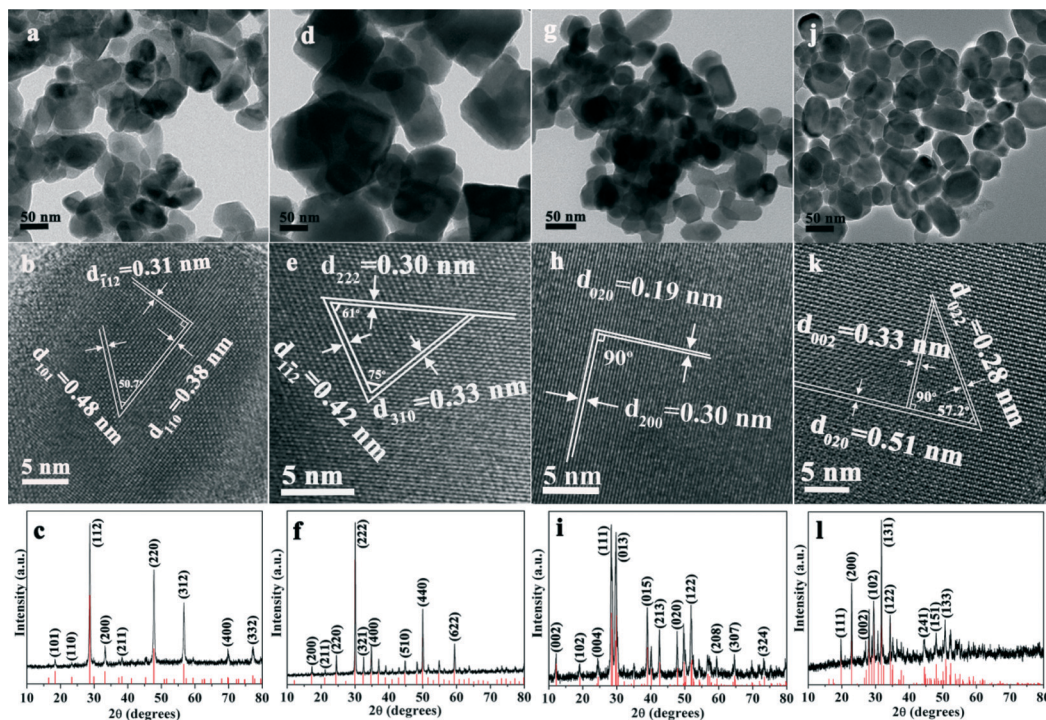


Fig. 1 TEM image, HRTEM image and XRD patterns of as-prepared (a–c) Cu_3SbS_4 nanocrystals; (d–f) $\text{Cu}_{12}\text{Sb}_4\text{S}_{13}$ nanocrystals; (g–i) CuSbS_2 nanocrystals; and (j–l) Cu_3SbS_3 nanocrystals.

of $\text{Cu}_{12}\text{Sb}_4\text{S}_{13}$, CuSbS_2 , and Cu_3SbS_3 NCs were obtained (Fig. S1†). With further increases in DDT to 20.5 mmol, the XRD result in Fig. 1i confirms the formation of orthorhombic CuSbS_2 NCs (PDF card No. 88-0822). In the HRTEM image (Fig. 1h), a lattice spacing of 0.30 nm was identified as the (200) plane, and a lattice spacing of 0.19 nm was indexed to the (020) plane perpendicular to the (200) plane. TEM images (Fig. 1g) of the as-prepared CuSbS_2 NCs show the tetragonal shape with an average size of 52 ± 8 nm. Phase-pure Cu_3SbS_3 NCs were obtained with further increases in the amount of DDT to 25.6 mmol. The peaks in Fig. 1l match well with the standard diffraction pattern of orthorhombic Cu_3SbS_3 (PDF card No. 88-1336). In the HRTEM image (Fig. 1k), clear lattice fringes with average interplanar distances of 0.28, 0.51, and 0.33 nm correspond to the (022), (020), and (002) planes of orthorhombic Cu_3SbS_3 , respectively. The TEM micrograph of Cu_3SbS_3 NCs shows the oval structure with an average size of 72 ± 5 nm.

Energy-dispersive X-ray spectroscopy (EDS) and XPS were conducted to confirm the compositions and phase structures. To acquire reliable data, quantitative EDS analysis at different locations was carried out. The nominal compositions for all four phases were found to be close to the expected ones (Fig. S2, ESI†). Interestingly, XPS analysis (Fig. S3–S6†) showed that the valence states of cations of all four phases were the same: for Cu is Cu(I) and Sb is Sb(III). For Cu_3SbS_4 nanocrystals, Sb(III) instead of Sb(V) had been previously found in the literature.⁷ For $\text{Cu}_{12}\text{Sb}_4\text{S}_{13}$ NCs, most of the reports reported that copper existed both in Cu(I) and Cu(II) oxidation states.³² However, the oxidation state of copper is still a matter of debate in bulk materials.^{36,37}

Apparently, the key factor on the composition and phase-controlled synthesis of Cu–Sb–S NCs was the amount of added DDT. In the synthesis of Cu-based chalcogenides, alkane thiols have been explored with various roles, such as surfactant, sulfur source, and solvent.^{38–40} To understand the composition and phase selectivity mechanism of Cu–Sb–S NCs, we investigated the role that DDT played in the synthesis first. In a contrast experiment, the stoichiometric amounts of $\text{Cu}(\text{Ac})_2$ and SbCl_3 , DDT, OA, and ODE were placed in a three-neck flask, cycled between vacuum and argon three times at 120 °C, and then heated at 200 °C for 1 h. XRD and TEM showed that the obtained products were ultrathin Cu_7S_4 nanosheets instead of Cu–Sb–S ternary NCs (Fig. 2). This result indicated that DDT was not a sulfur source for the growth of Cu–Sb–S NCs. We have noted that SbCl_3 does not react with DDT to produce Sb_2S_3 or Sb_2S_5 , even when the reaction temperature reaches at 278 °C. Generally, DDT is introduced as a reactivity controlling ligand in the synthesis of Cu-based multicomponent chalcogenides.^{41,42} According to the hard–soft acid–base theory, Cu^+ is a soft Lewis acid and Sb^{3+} is an intermediate Lewis acid. Therefore, the S precursor, being as soft Lewis base, will be more reactive to Cu^+ than to Sb^{3+} . After the adding of DDT, strong binding of DDT to Cu^+ ions give rise to a relatively slow reaction of the copper ions with the chalcogens. By this, phase selective synthesis may be involved in the relative reaction rates between different metal precursors and S precursors. By reducing the Cu precursor ratios, the relative reaction rate between Cu precursor and S precursor decreases. However, composition and phase-controlled synthesis of Cu–Sb–S NCs was not achieved (Fig. S7†). When the added amount of DDT was fixed and the

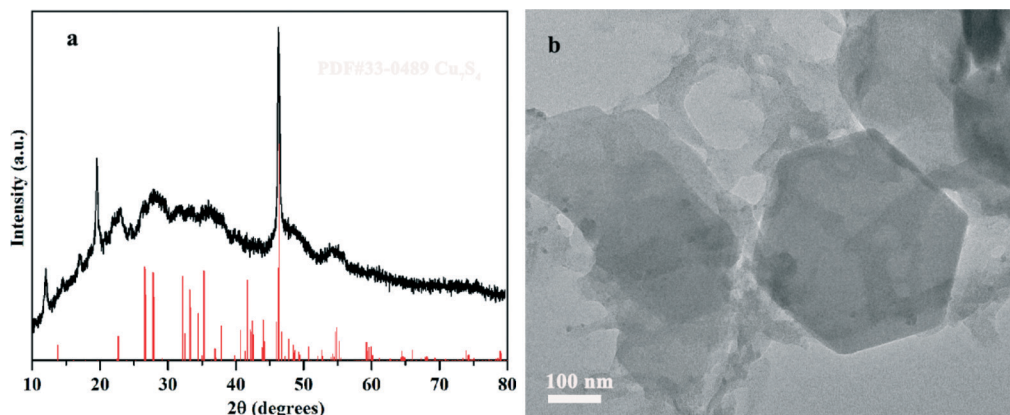


Fig. 2 (a) XRD and (b) TEM image of Cu_7S_4 nanosheets obtained by heating stoichiometric amounts of $\text{Cu}(\text{Ac})_2$, SbCl_3 , and DDT at $200\text{ }^\circ\text{C}$ for 1 h.

Cu/Sb precursor ratios were systematically changed from 1:0.3 to 1:2, all of the products were phase-pure Cu_3SbS_4 NCs. Further increasing the Sb precursor ratios just lead to the formation of Sb_2S_3 impurities. Thus, the role of DDT was more than a reactivity-controlling ligand in the growth of Cu-Sb-S NCs.

To further obtain insight into the role of DDT and the phase selectivity mechanism, experiments on the formation pathway of these NCs were performed. Several works^{4,43,44} have indicated that the growth of the copper-based ternary (I–III–VI) or quaternary (I–II–IV–VI) NCs roots generally from the insertion of the III or II, IV cations into the pre-formed binary Cu_{2-x}S seeds. However, in the case of Cu-Sb-S NCs, the issue may be different. When $\text{Cu}(\text{Ac})_2$ and DDT were heated at $200\text{ }^\circ\text{C}$ for 30 min, small Cu_2S seeds were prepared (Fig. S8a and S8b[†]). Injection of SbCl_3 in OA and ODE solution followed by heating the mixture at $200\text{ }^\circ\text{C}$ for 1 h did not result in any Cu-Sb-S NCs; however, larger Cu_2S NCs were formed (Fig. S8a and S8c[†]). When we separately prepared Cu_2S and Sb_2S_3 NCs, and then inject them together with heating at $200\text{ }^\circ\text{C}$ for 1 h, pure Cu_3SbS_3 NCs were obtained (Fig. 3). While for the Cu_7S_4 and Sb_2S_3 counterparts, $\text{Cu}_{12}\text{Sb}_4\text{S}_{13}$ and Cu_3SbS_3 mixed-phase NCs were formed (Fig. S9[†]). Based on these results, we concluded that the formation of Cu-Sb-S NCs may relate to the reaction of Sb_2S_3 with different Cu_{2-x}S seeds. In other words, the for-

mation pathway of Cu-Sb-S NCs was possible by the reaction: $\text{Cu}_{2-x}\text{S} + \text{Sb}_2\text{S}_3 \rightarrow \text{Cu-Sb-S}$ NCs.

Based on this formation pathway, we discuss the influence of the amounts of DDT on the Cu_{2-x}S and Sb_2S_3 seeds, respectively. $\text{Cu}(\text{Ac})_2$, or SbCl_3 , in different amounts of DDT respectively, react with the sulfur precursor. For SbCl_3 , regardless of the amount of DDT added, the obtained NCs are always orthorhombic Sb_2S_3 (Fig. S10[†]). However, for $\text{Cu}(\text{Ac})_2$, the amount of DDT does greatly influence the composition and crystal structure of the formed Cu_{2-x}S NCs (Fig. 4). When the amount of DDT is 0.7, 2, 9.5, and 10 mL, hexagonal CuS , cubic $\text{Cu}_{7.2}\text{S}_4$, monoclinic $\text{Cu}_{31}\text{S}_{16}$, and hexagonal Cu_2S NCs are obtained, respectively. A similar phenomenon has also been observed in the literature.^{45,46} Plass *et al.*⁴⁶ recently reported that alteration of the DDT/OA solvent ratio lead to the preparation of a variety of different copper sulfides with varying compositions and crystal structures (CuS , $\text{Cu}_{1.8}\text{S}$, $\text{Cu}_{1.96}\text{S}$, and Cu_2S). The phase selectivity of copper sulfides was attributed to different precursor speciation, which originated from the different reducing ability of DDT *versus* OA. Therefore, in our systems, DDT not only acted as a reactivity controlling ligand, but also as the controller of reducing ability. The different DDT amounts lead to different reducing conditions, thereby resulting in the formation of different compositions and crystal structures of Cu_{2-x}S seeds.

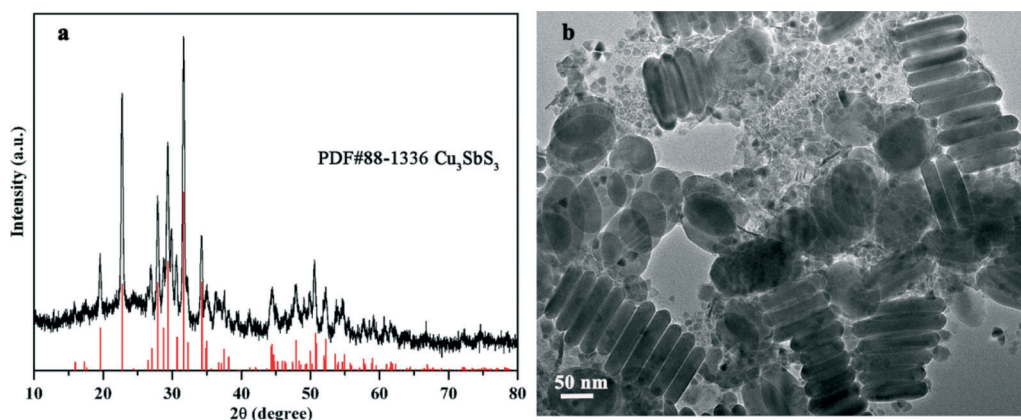


Fig. 3 (a) XRD and (b) TEM image of nanocrystals synthesized with Cu_2S and Sb_2S_3 as seeds at $200\text{ }^\circ\text{C}$ for 1 h.

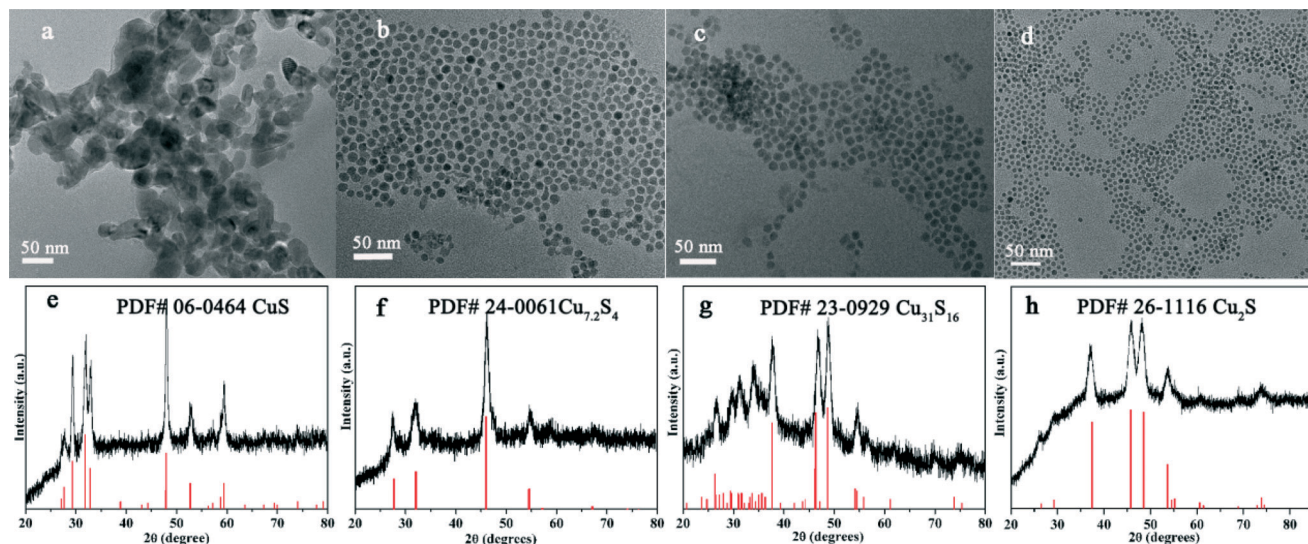


Fig. 4 TEM images and XRD of Cu_{2-x}S nanocrystals with different amounts of DDT: (a, e) 0.7 mL; (b, f) 2 mL; (c, g) 9.5 mL; and (d, h) 10 mL.

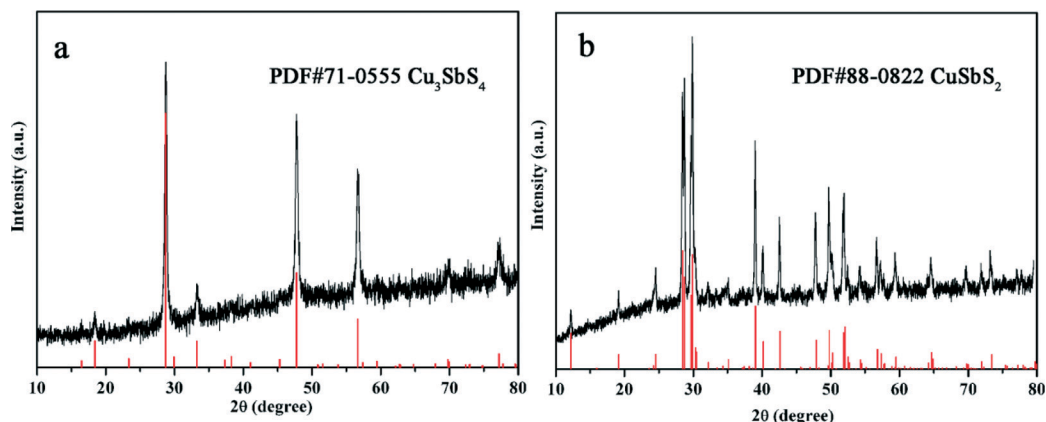


Fig. 5 XRD patterns of nanocrystals synthesized with (a) CuS and Sb_2S_3 as seeds at 200 °C for 1 h; (b) $\text{Cu}_{31}\text{S}_{16}$ and Sb_2S_3 as seeds at 200 °C for 1 h.

The formed Cu_{2-x}S seeds reacted with Sb_2S_3 NCs, resulting in different compositions and phase structures of Cu–Sb–S NCs. That is, the composition and phase-controlled synthesis of Cu–Sb–S NCs was determined by the initial Cu_{2-x}S seeds.

To confirm this mechanism, we synthesized Cu–Sb–S NCs by the reaction of Sb_2S_3 NCs with CuS or $\text{Cu}_{31}\text{S}_{16}$ NCs at 200 °C for 1 h, respectively. Fig. 5 shows the XRD patterns of pure-phase Cu_3SbS_4 and CuSbS_2 NCs, respectively, illustrating the composition and phase-controlled synthesis.

In the literature,^{22,32,34} both the type and the amount of sulfur sources were found to be significantly important to the phase-selective synthesis of Cu–Sb–S NCs. Yet the substantial role of the sulfur source has not been explored. By changing the reactivity of sulfur precursors, we discuss the effect of sulfur source on the composition and phase-controlled synthesis of Cu–Sb–S NCs. It has been known that the reactivity of sulfur precursors can be controlled by the heating temperature and reaction time.⁴⁷ High temperature converts the S_8 rings to polysulfides with long S chains and promotes the breakage of the long S chains, making the sulfur precursors more active. As shown in Fig. 6, when elemental sulfur in 1-octadecene heated

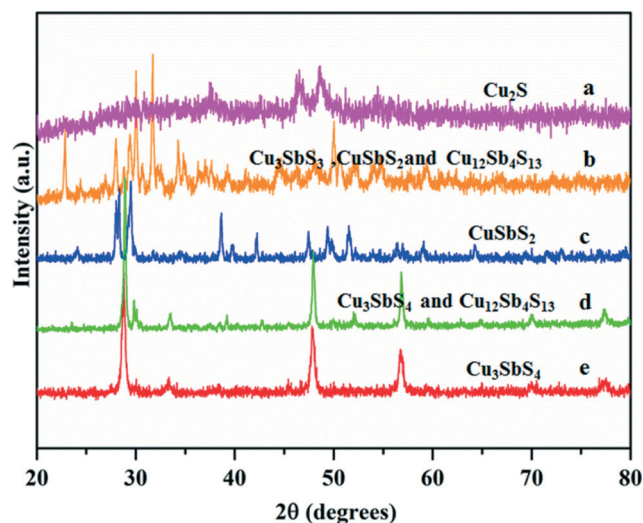
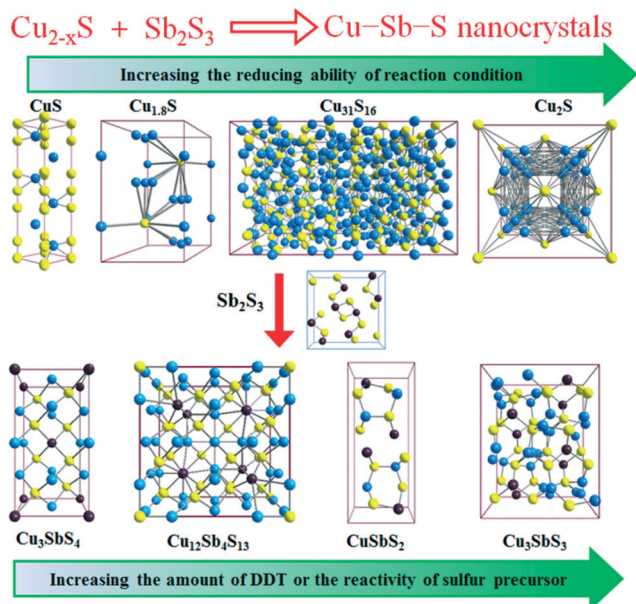


Fig. 6 XRD patterns of nanocrystals synthesized with different reactivity of sulfur precursors prepared by heating at (a) 240 °C; (b) 200 °C; (c) 180 °C; (d) 150 °C; and (e) 120 °C for 20 min.



Scheme 1 Schematic for composition and phase-controlled synthesis of Cu-Sb-S nanocrystals. The composition and phase-controlled synthesis of Cu-Sb-S nanocrystals is determined by the initial Cu_{2-x}S seeds. Different compositions, and crystal structures of Cu_{2-x}S seeds results in different compositions and phase structures of Cu-Sb-S nanocrystals.

to 120 °C for 20 min, Cu_3SbS_4 NCs are obtained. While with further increase in temperature to 150 °C; 180 °C; and 200 °C, mixed-phases of Cu_3SbS_4 and $\text{Cu}_{12}\text{Sb}_4\text{S}_{13}$; pure CuSbS_2 ; and mixed-phases of $\text{Cu}_{12}\text{Sb}_4\text{S}_{13}$, CuSbS_2 , and Cu_3SbS_3 NCs are obtained, respectively. Further increases in temperature leads to the formation of Cu_2S NCs instead of Cu-Sb-S ternary NCs. The reactivity of sulfur precursors also does have a significant effect on phase-selective synthesis of Cu-Sb-S NCs. To explore the role of the sulfur source, we investigated the effect of the reactivity of sulfur precursors on the Cu_{2-x}S and Sb_2S_3 seeds, respectively. Similar to the amount of DDT, the different reactivity of sulfur precursors does not have a noticeable impact on the Sb_2S_3 seeds, but they do result in different compositions and crystal structures of Cu_{2-x}S NCs. When the other reaction parameters are fixed and the reactivity of sulfur precursors is changed with heating at 150 °C and 200 °C for 20 min, the obtained Cu_{2-x}S NCs are hexagonal CuS and Cu_2S (Fig. S11, ESI[†]), respectively. These results further confirm that phase-selective synthesis of Cu-Sb-S NCs is determined by the initial Cu_{2-x}S seeds. When the reactivity of the sulfur precursor, or the DDT amount is changed, different compositions and crystal structures of Cu_{2-x}S seeds are formed because of the different reducing abilities of the systems. A clear formation path of Cu-Sb-S NCs is demonstrated in Scheme 1. Different compositions and phase structure of Cu-Sb-S NCs are obtained by the reaction of the Cu_{2-x}S seeds with Sb_2S_3 seeds.

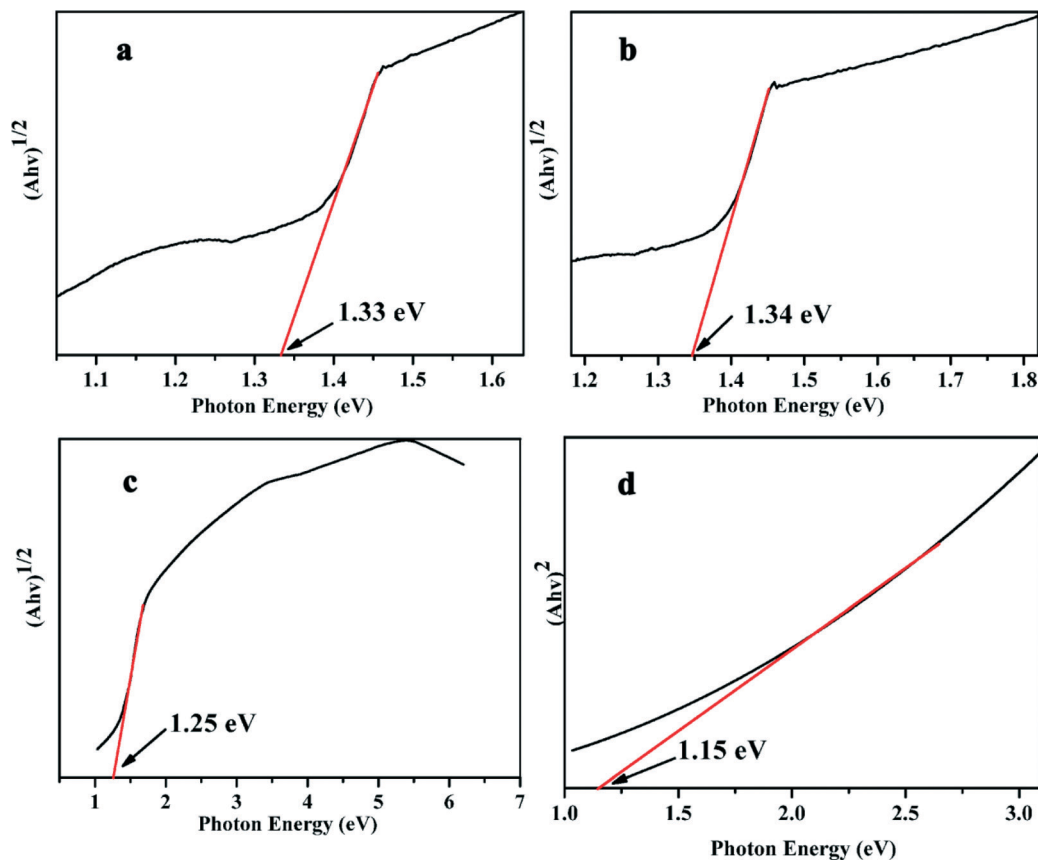


Fig. 7 Extrapolation of the absorption spectra in the band edge region for the determination of band gaps of the as-prepared (a) Cu_3SbS_4 , (b) $\text{Cu}_{12}\text{Sb}_4\text{S}_{13}$, (c) CuSbS_2 , and (d) Cu_3SbS_3 nanocrystals.

The optical properties of the as-synthesized phase-pure Cu–Sb–S NCs were investigated by UV-vis-NIR absorption spectroscopy (Fig. S12, ESI[†]). The optical band gaps were estimated by using the method based on the relationship of $(\alpha h\nu)^n$ versus $h\nu$ (where α is absorbance, h is Planck's constant, and ν is frequency, $n = 2$ or $1/2$). The results (Fig. 7) show that all of the Cu₃SbS₄, Cu₁₂Sb₄S₁₃, and CuSbS₂ NCs were indirect band gap semiconductors with band gaps of ~ 1.33 , ~ 1.34 , and ~ 1.25 eV, respectively; while for Cu₃SbS₃ NCs, the direct band gap was 1.15 eV. The band gap value and direct absorption nature of the as-prepared Cu₃SbS₃ NCs were in good agreement with previous reports^{19,22,24} and make them attractive candidates for the application of solar energy conversion. CuSbS₂ has been found as an indirect band gap semiconductor in theoretical calculations,¹⁷ however, experimental results for CuSbS₂ have reported it to be both a direct and indirect band gap material.^{33,35} The band gap value and indirect behavior of the CuSbS₂ NCs in our results are consistent with the theoretical study. Because of the large size of the obtained NCs, no quantum confinement effect was observed, and thus, their indirect bands were all in good agreement with the previous reports of bulk Cu₃SbS₄, Cu₁₂Sb₄S₁₃.^{48,49}

Conclusion

In this work, composition and phase-controlled synthesis of Cu–Sb–S NCs are performed by a facile hot-injection procedure. While fixing the other parameters, by only changing the amount of DDT, a series of pure tetragonal Cu₃SbS₄, cubic Cu₁₂Sb₄S₁₃, orthorhombic CuSbS₂, and orthorhombic Cu₃SbS₃ NCs are obtained. A systematic investigation shows that the DDT not only acts as reactivity controlling ligand, but also as the controller of reducing ability. Different amounts of DDT leads to the different reducing conditions. As a result, different compositions and crystal structures of Cu_{2-x}S seeds are formed. The reactions of Sb₂S₃ NCs with different Cu_{2-x}S seeds reveal that the composition and phase-controlled synthesis of Cu–Sb–S NCs is determined by the initial Cu_{2-x}S seeds. Furthermore, the phase structures of Cu_{2-x}S seeds can also be affected by the reactivity of the sulfur precursor. This scenario will lead to the phase selective synthesis of Cu–Sb–S NCs. This phase selectivity mechanism may have positive implications on other I–V–VI multicomponent chalcogenides NCs such as the Cu–Bi–S system.

Acknowledgements

This work was supported by the National Natural Science Foundation of China (Grants 21427802, 21131002 and 21201075) and the Specialized Research Fund for the Doctoral Program of Higher Education (SRFDP Grant 20110061130005). Wei Zhang is supported by the Open Foundation from State Key Laboratory of Inorganic Synthesis and Preparative Chemistry (2016-09).

References

- 1 A. Singh, A. Singh, J. Ciston, K. Bustillo, D. Nordlund and D. J. Milliron, *J. Am. Chem. Soc.*, 2015, **137**, 6464–6467.
- 2 Q. Tian, G. Wang, W. Zhao, Y. Chen, Y. Yang, L. Huang and D. Pan, *Chem. Mater.*, 2014, **26**, 3098–3103.
- 3 Y. X. Wang, M. Wei, F. J. Fan, T. T. Zhuang, L. Wu, S. H. Yu and C. F. Zhu, *Chem. Mater.*, 2014, **26**, 5492–5498.
- 4 J. J. Wang, P. Liu, C. C. Seaton and K. M. Ryan, *J. Am. Chem. Soc.*, 2014, **136**, 7954–7960.
- 5 W. C. Yang, C. K. Miskin, N. J. Carter, R. Agrawal and E. A. Stach, *Chem. Mater.*, 2014, **26**, 6955–6962.
- 6 X. Yu, A. Shavel, X. An, Z. Luo, M. Ibanez and A. Cabot, *J. Am. Chem. Soc.*, 2014, **136**, 9236–9239.
- 7 J. van Embden and Y. Tachibana, *J. Mater. Chem.*, 2012, **22**, 11466.
- 8 C. Yan, Z. Su, E. Gu, T. Cao, J. Yang, J. Liu, F. Liu, Y. Lai, J. Li and Y. Liu, *RSC Adv.*, 2012, **2**, 10481.
- 9 K. Ramasamy, H. Sims, W. H. Butler and A. Gupta, *J. Am. Chem. Soc.*, 2014, **136**, 1587–1598.
- 10 W. Septina, S. Ikeda, Y. Iga, T. Harada and M. Matsumura, *Thin Solid Films*, 2014, **550**, 700–704.
- 11 B. Yang, L. Wang, J. Han, Y. Zhou, H. Song, S. Chen, J. Zhong, L. Lv, D. Niu and J. Tang, *Chem. Mater.*, 2014, **26**, 3135–3143.
- 12 K. Ramasamy, R. K. Gupta, S. Palchoudhury, S. Ivanov and A. Gupta, *Chem. Mater.*, 2015, **27**, 379–386.
- 13 S. Suehiro, K. Horita, M. Yuasa, T. Tanaka, K. Fujita, Y. Ishiwata, K. Shimano and T. Kida, *Inorg. Chem.*, 2015, **54**, 7840–7845.
- 14 Y. C. Choi, E. J. Yeom, T. K. Ahn and S. I. Seok, *Angew. Chem., Int. Ed.*, 2015, **54**, 4005–4009.
- 15 W.-L. Chen, D.-H. Kuo and T. T. A. Tuan, *J. Electron. Mater.*, 2015, **45**, 688–694.
- 16 H. Guo, Y. Cui, Q. Tian, S. Gao, G. Wang and D. Pan, *Cryst. Growth Des.*, 2015, **15**, 771–777.
- 17 D. J. Temple, A. B. Kehoe, J. P. Allen, G. W. Watson and D. O. Scanlon, *J. Phys. Chem. C*, 2012, **116**, 7334–7340.
- 18 J. T. Dufton, A. Walsh, P. M. Panchmatia, L. M. Peter, D. Colombara and M. S. Islam, *Phys. Chem. Chem. Phys.*, 2012, **14**, 7229–7233.
- 19 A. B. Kehoe, D. J. Temple, G. W. Watson and D. O. Scanlon, *Phys. Chem. Chem. Phys.*, 2013, **15**, 15477–15484.
- 20 M. Kumar and C. Persson, *Energy Procedia*, 2014, **44**, 176–183.
- 21 T. Shi, W. J. Yin, M. Al-Jassim and Y. Yan, *Appl. Phys. Lett.*, 2013, **103**, 152105.
- 22 K. Ramasamy, H. Sims, W. H. Butler and A. Gupta, *Chem. Mater.*, 2014, **26**, 2891–2899.
- 23 C. Tablero, *J. Phys. Chem. C*, 2014, **118**, 15122–15127.
- 24 Z. Hao, D. Zeng, L. Chen and F. Huang, *Mater. Lett.*, 2014, **122**, 338–340.
- 25 Z. Jiasong, X. Weidong, J. Huaidong, C. Wen, L. Lijun, Y. Xinyu, L. Xiaojuan and L. Haitao, *Mater. Lett.*, 2010, **64**, 1499–1502.
- 26 F. L. Skinner and E. Makovicky, *Econ. Geol.*, 1972, **67**, 924–938.
- 27 S. V. Kershaw, A. S. Sussha and A. L. Rogach, *Chem. Soc. Rev.*, 2013, **42**, 3033.
- 28 D. Aldakov, A. Lefrançois and P. Reiss, *J. Mater. Chem. C*, 2013, **1**, 3756.
- 29 R. Rodriguez, M. P. Hendricks, B. Cossairt, H. Liu and J. S. Owen, *Chem. Mater.*, 2013, **25**, 1233–1249.
- 30 S. Mourdikoudis and L. M. Liz-Marzán, *Chem. Mater.*, 2013, **25**, 1465–1476.

- 31 Y. W. Jun, J. S. Choi and J. Cheon, *Angew. Chem., Int. Ed.*, 2006, **45**, 3414–3439.
- 32 J. van Embden, K. Latham, N. W. Duffy and Y. Tachibana, *J. Am. Chem. Soc.*, 2013, **135**, 11562–11571.
- 33 D. Xu, S. Shen, Y. Zhang, H. Gu and Q. Wang, *Inorg. Chem.*, 2013, **52**, 12958–12962.
- 34 S. Ikeda, S. Sogawa, Y. Tokai, W. Septina, T. Harada and M. Matsumura, *RSC Adv.*, 2014, **4**, 40969–40972.
- 35 Y. Zou and J. Jiang, *Mater. Lett.*, 2014, **123**, 66–69.
- 36 F. Di Benedetto, G. P. Bernardini, C. Cipriani, C. Emiliani, D. Gatteschi and M. Romanelli, *Phys. Chem. Miner.*, 2005, **32**, 155–164.
- 37 A. N. Buckley, W. M. Skinner, S. L. Harmer, A. Pring, R. N. Lamb, L. J. Fan and Y. W. Yang, *Can. J. Chem.*, 2007, **85**, 767–781.
- 38 L. Li, A. Pandey, D. J. Werder, B. P. Khanal, J. M. Pietryga and V. I. Klimov, *J. Am. Chem. Soc.*, 2011, **133**, 1176–1179.
- 39 L. Li, J. Daou, I. Texier, T. Chi, N. Liem and P. Reiss, *Chem. Mater.*, 2009, **21**, 2422–2429.
- 40 Z. Liu, L. Wang, Q. Hao, D. Wang, K. Tang, M. Zuo and Q. Yang, *CrystEngComm*, 2013, **15**, 7192.
- 41 R. Xie, M. Rutherford and X. Peng, *J. Am. Chem. Soc.*, 2009, **131**, 5691–5697.
- 42 Q. Liang, L. Han, X. Deng, C. Yao, J. Meng, X. Liu and J. Meng, *CrystEngComm*, 2014, **16**, 4001.
- 43 L. De Trizio, H. Li, A. Casu, A. Genovese, A. Sathya, G. C. Messina and L. Manna, *J. Am. Chem. Soc.*, 2014, **136**, 16277–16284.
- 44 J. M. Tan, Y. H. Lee, S. Pedireddy, T. Baikie, X. Y. Ling and L. H. Wong, *J. Am. Chem. Soc.*, 2014, **136**, 6684–6692.
- 45 A. M. Wiltrout, N. J. Freymeyer, T. Machani, D. P. Rossi and K. E. Plass, *J. Mater. Chem.*, 2011, **21**, 19286.
- 46 N. J. Freymeyer, P. D. Cunningham, E. C. Jones, B. J. Golden, A. M. Wiltrout and K. E. Plass, *Cryst. Growth Des.*, 2013, **13**, 4059–4065.
- 47 Y. Zou, X. Su and J. Jiang, *J. Am. Chem. Soc.*, 2013, **135**, 18377–18384.
- 48 N. D. Franzer, N. R. Paudel, C. Xiao and Y. Yan, *2014 Ieee 40th Photovoltaic Specialist Conference (Pvsc)*, Ieee, 2014, pp. 2326–2328.
- 49 L. Wang, B. Yang, Z. Xia, M. Leng, Y. Zhou, D. J. Xue, J. Zhong, L. Gao, H. Song and J. Tang, *Sol. Energy Mater. Sol. Cells*, 2016, **144**, 33–39.